# Influence of Dissolved Hydrogen on the Intergranular Oxidation Behaviour of Ni-based Alloys in Simulated PWR Primary Water

Yun Soo Lim*, Sung Woo Kim, Dong Jin Kim, Hong Pyo Kim, Jong Yeon Lee
*Materials Safety Technology Development Division/Korea Atomic Energy Research Institute*
*1045 Daedeok-daero, Yuseong-gu, Daejeon 305-353, Korea*
**Corresponding author: yslim@kaeri.re.kr*

## 1. Introduction

Primary water stress corrosion cracking (PWSCC) of Ni-based Alloy 600 has been a major concern in the primary side of pressurized water reactors (PWRs). In response to the cracking problems associated with Alloy 600, another solid-solution strengthened Ni-based alloy, Alloy 690, has become the common replacement material in PWR service. Alloy 690 is known to be more resistant to PWSCC than Alloy 600 [1]. Recently, the internal oxidation theory as a possible IGSCC mechanism for Ni-based alloys has attracted much attention. Two types of changes occur in Ni-based alloys owing to the inward solid-state diffusion of oxygen. Oxygen reacts selectively with the solute metal Cr beneath the surface to form discrete Cr-rich oxide particles via a process referred to as 'internal oxidation'. The surface grain boundaries are also oxidized by oxygen penetration along the grain boundaries and by short-circuit outward diffusion of Cr at the grain boundaries, resulting in grain boundary oxidation, which is referred to as 'IG oxidation' [2]. Dissolved hydrogen is known to have significant effects on the cracking behavior of Ni-based alloys. The PWSCC susceptibilities of Alloy 600 and its weld metals are known to peak near the Ni/NiO transition [3].

The aim of the present study was to characterize the internal and IG oxidation phenomena depending on the hydrogen concentration to obtain clear insight into the role of dissolved hydrogen on the different resistance to PWSCC of Alloys 600 and 690 when exposed to PWR primary water. After the test, the microchemical changes near the surface and around the grain boundaries due to oxygen diffusion were precisely characterized using various types of microscopic equipment, in this case, scanning electron microscopy (SEM), TEM, and fine-probe chemical analysis using energy dispersive X-ray spectroscopy (EDS) in the scanning TEM (STEM) mode. Finally, possible correlations between the internal and IG oxidation and the dissolved hydrogen are discussed based on the observed results.

## 2. Methods

### *2.1. Materials*

A mill-annealed Alloy 600 round bar with an outside diameter of 120 mm was used in this study. The Alloy 600 round bar was finally heat-treated at 950 ℃ for 3 hours and quenched with water. A forged round bar of Alloy 690 with an outside diameter of 196 mm was also used. The Alloy 690 round bar was finally solution-annealed and quenched with water. Alloys 600 and 690 used in this study were archive materials for control rod drive mechanism (CRDM) penetration nozzles for use in a PWR. Detailed information on the chemical compositions, microstructures and cracking behavior of the test alloys are described in the literature [4].

### *2.2. Oxidation Test*

Coupons (10×10×2 $mm^3$) cut from the round bar were prepared by grinding with SiC paper to a 2000 mesh and subsequently polishing with alumina powders down to 0.3 ㎛. The simulated PWR water was prepared prior to the test in a storage tank. 1200 ppm B (by weight) of $H_3BO_3$ and 2 ppm Li (by weight) of Li(OH) were added to pure water. After the removal of the dissolved oxygen by purging with nitrogen gas, hydrogen was added to the simulated PWR primary water. The oxygen concentration was maintained at less than 5 ppb during the test. The specimens were exposed to simulated primary water at hydrogen concentrations of 5 and 30 $cm^3$ $H_2$/kg $H_2O$ for a period of 3600 hours. The test temperature was 325 ℃. The combinations of the temperature and the hydrogen concentration used for the present study correspond to the conditions where Ni is in the oxidized state (5 $cm^3$ $H_2$/kg $H_2O$), and Ni is in the metallic state (30 $cm^3$ $H_2$/kg $H_2O$) [3].

### *2.3. TEM Analysis*

TEM specimens from the oxidized coupons were prepared by performing a standard lift-out procedure using a focused ion beam (FIB) milling technique. A dual-beam Hitachi FIB-2100 system was used to prepare cross-sectional TEM specimens with $Ga^+$ ion sputtering to characterize the internal oxidation layer and the IG penetration of oxygen at the grain boundaries. Thinning of the specimens to electron transparency was conducted using $Ga^+$ ions at successively lower beam energy levels of 30, 10, and 5 kV. A conventional TEM analysis of the crystallography was conducted with a JEOL JEM-2100F (operating voltage 200 kV). Composition mapping around oxidation layers was performed on an STEM EDS with a JEOL JEM-2100F (operating voltage 200 kV) equipped with an Oxford Instruments X-max80T Silicon Drift Detector with a

solid angle of 0.2361 steradian and an AZtec analysis system (Ver. 3.1b).

## 3. Results

### *3.1. Internal and Intergranular Oxidation of Alloy 600*

Fig. 1 was obtained from Alloy 600 at a hydrogen concentration of 30 $cm^3$ $H_2$/kg $H_2O$ tested at 325 ℃ for a period of 3600 hrs, presenting a STEM image and EDS spectrum images of O, Cr, Fe, and Ni obtained using the Kα1 lines around the surface. A grain boundary is visible in the STEM image. In the O spectrum image, a continuous thin Cr-rich oxide layer appears to emerge. The faceted oxides over the surface grain boundary were identified as (Ni,Fe) spinel. The most intriguing feature in Fig. 1 is that oxygen diffused down along the grain boundary, causing the grain boundary to be oxidized. Due to the diffusion of oxygen, Cr oxide formed in the oxidized grain boundary. Ni was enriched inside the oxidized grain boundary near the surface. Lim et al. [2] also observed highly Ni-enriched regions around the interface between a Cr carbide and the oxidized grain boundary under the same experimental conditions. Therefore, the formation of Ni-enriched regions is very common during the IG oxidation process of Alloy 600 in primary water whenever oxygen penetrates the metal and Cr is internally oxidized to form an oxide. This behavior of Ni is thought to be mainly attributable to Ni being in a metallic state at this hydrogen concentration.

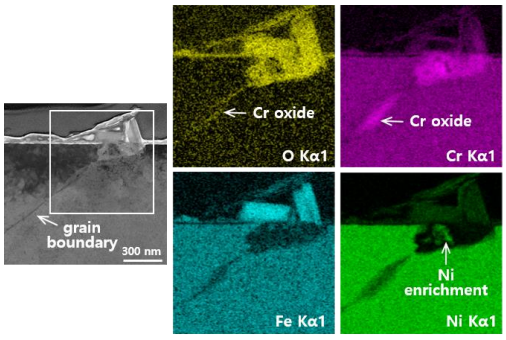


Fig. 1. STEM image and EDS spectrum images of O, Cr, Fe, and Ni around the surface of Alloy 690 at a hydrogen concentration of 30 $cm^3$ $H_2$/kg $H_2O$ tested at 325 ℃.

Fig. 2 shows a STEM image and EDS spectrum images of O, Cr, Fe, and Ni around the surface obtained from Alloy 600 at a hydrogen concentration of 5 $cm^3$ $H_2$/kg $H_2O$ tested at 325 ℃ for a period of 3600 hrs. First, the faceted oxide on the surface was identified as (Ni,Fe) spinel with a minor amount of Cr and the filamentary oxides beneath the (Ni,Fe) spinel were identified as Ni-rich oxides from EDS measurement. IG oxidation also occurred at this hydrogen concentration.

Therefore, it appears that IG oxidation commonly occurs in Alloy 600 irrespective of the hydrogen concentration. The noticeable difference in IG oxidation between Figs. 1 and 2 is that, while Ni was enriched in the oxidized grain boundary when Ni was in a reduced state at a hydrogen concentration of 30 $cm^3$ $H_2$/kg $H_2O$, Ni reacted with diffusing oxygen, resulting in the formation of Ni-rich oxides in the oxidized grain boundary when Ni was in an oxidized state at a hydrogen concentration of 5 $cm^3$ $H_2$/kg $H_2O$.

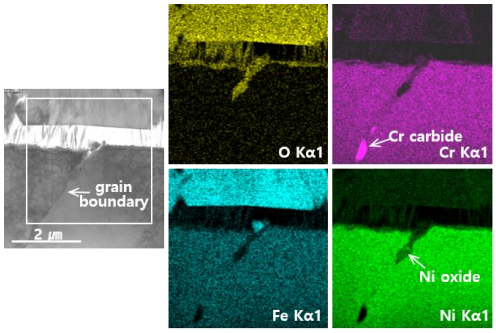


Fig. 2. STEM image and EDS spectrum images of O, Cr, Fe, and Ni around the surface of Alloy 600 at a hydrogen concentration of 5 $cm^3$ $H_2$/kg $H_2O$ tested at 325 ℃.

### *3.1. Internal and Intergranular Oxidation of Alloy 600*

Fig. 3 shows a STEM image and EDS spectrum images of O, Cr, Fe and Ni around the surface obtained from Alloy 690 at a hydrogen concentration of 30 $cm^3$ $H_2$/kg $H_2O$ tested at 325 ℃ for a period of 3600 hrs. The surgace oxidation layers were much thicker than those of Alloy 600 under the same experimental conditions, as confirmed from the O spectrum images in Figs. 1 and 2.

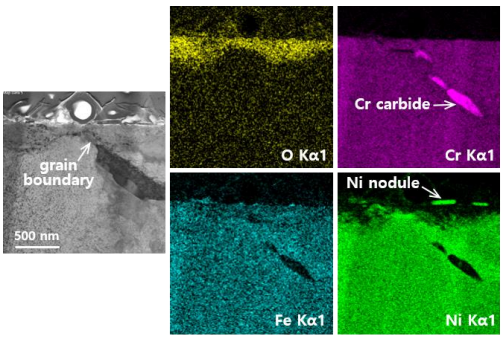


Fig. 3. STEM image and EDS spectrum images of O, Cr, Fe, and Ni around the surface of Alloy 690 at a hydrogen concentration of 30 $cm^3$ $H_2$/kg $H_2O$ tested at 325 ℃.

The most noticeable feature in this figure is that there is no oxygen diffusion along a grain boundary that indicates that IG oxidation did not occur, in contrast with Alloy 600 of Fig. 1. Ni nodules are visible on the surface, which is similar to the Ni enrichment in the oxidized grain boundary of Fig. 1. From these results, it can be confirmed that the IG oxidation phenomena of Alloy 690 were quite different from those of Alloy 600.

The main reason for these differences is thought to be the different chemical compositions, especially the different Cr contents in these two alloy groups. Lim et al. [5] revealed that a protective innermost $Cr_2O_3$ layer formed through the grain boundary diffusion of Cr and it prevented oxygen from diffusing into a grain boundary resulting in the suppression of IG oxidation of Alloy 690 due to a high Cr content of approximately 30 wt% in this alloy.

Fig. 4 was obtained from Alloy 690 at a hydrogen concentration of 5 $cm^3$ $H_2$/kg $H_2O$ tested at 325 ℃ for a period of 3600 hrs. The intriguing features in this figure are that diffusion induced grain boundary migration (DIGM) occurred, and the oxidation layer along the surface swept by DIGM was considerably thin compared to the surrounding layer. As shown in Fig. 4, the grain boundary migration zone was highly enriched in Ni and depleted in Cr. It means that the migration process was caused by DIGM as it was related to the diffusion of solute. Interestingly, there is a Ni-rich region on the swept grain boundary. Recently, DIGM in Ni-based alloys during exposure to simulated PWR primary water or hydrogenated steam has been reported as a commonly occurring process [6,7], and DIGM has been an attractive research subject in terms of IG oxidation and cracking owing to the accompanying Cr depletion. When dynamic straining is applied, successive cycles of surface oxide film rupture and repair deplete Cr at the grain boundary. Hence, an IG crack can initiate when the Cr-depleted grain boundary is no longer able to support the formation of a protective Cr oxide layer. Therefore, it has been argued that DIGM and IG oxidation are two important precursors of the IGSCC process of Alloy 690 [6,7]. IG oxidation was not visible at this hydrogen concentration as in the case of the hydrogen concentration of 30 $cm^3$ $H_2$/kg $H_2O$.

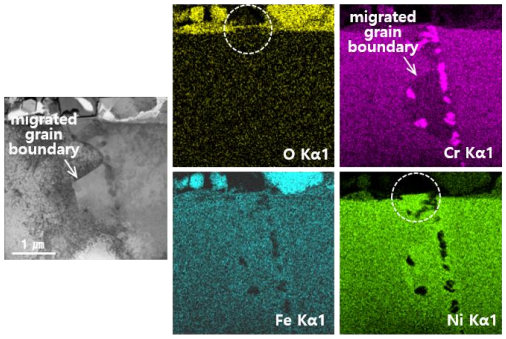


Fig. 4. STEM image and EDS spectrum images of O, Cr, Fe, and Ni around the surface of Alloy 690 at a hydrogen concentration of 5 $cm^3$ $H_2$/kg $H_2O$ tested at 325 ℃.

## 4. Conclusions

In the present study, the internal and IG oxidation phenomena in Alloys 600 and 690 depending on the hydrogen concentration were characterized to obtain clear insight into the different resistance to PWSCC and the cracking behavior when exposed to PWR primary water. It was revealed from a TEM examination that surface grain boundaries were oxidized in Alloy 600 within a range of hydrogen concentration between 5 and 30 $cm^3$ $H_2$/kg $H_2O$. There was Ni enrichment in the oxidized regions of Alloy 600 when the hydrogen concentration was 30 $cm^3$ $H_2$/kg $H_2O$, whereas Ni-rich oxides emerged in the oxidized regions when the hydrogen concentration was 5 $cm^3$ $H_2$/kg $H_2O$. This indicates that the behavior of Ni in Alloy 600 considerably changes depending on the hydrogen concentration. On the other hand, IG oxidation did not occur in Alloy 690 within a range of hydrogen concentration between 5 and 30 $cm^3$ $H_2$/kg $H_2O$. Ni nodules emerged on the surface when the hydrogen concentration was 30 $cm^3$ $H_2$/kg $H_2O$. Therefore, it appears that the formation of Ni nodules or Ni enrichment is common in Ni-based alloys when Ni is in a reduction state. DIGM commonly occurred in Alloy 690 irrespective of the hydrogen concentration. All the above different oxidation phenomena observed in Alloys 600 and 690 depending on the hydrogen concentration are believed to significantly affect their resistance to PWSCC.

## REFERENCES

[1] G. A. White and J. Hickling, L. K. Mathews, Crack growth rates for evaluating PWSCC of thick-wall Alloy 600 material, Proc. of the 11th Int. Conf. on Environmental Degradation of Materials in Nuclear Power Systems-Water Reactor (Stevenson, WA: TMS), pp. 166-179, 2003.
[2] Y.S. Lim, S.W. Kim, S.S. Hwang, H.P. Kim and C. Jang, Intergranular oxidation of Ni-based Alloy 690 in a simulated PWR primary water environment, Corros. Sci. Vol. 108, pp. 125-133, 2016.
[3] S.A. Attanasio and D.S. Morton, Measurement of the Nickel/Nickel Oxide Transition in Ni-Cr-Fe Alloys and Updated Data and Correlations to Quantify the Effect of Aqueous Hydrogen on Primary Water SCC, Proc. of the 11th Int. Conf. on Environmental Degradation of Materials in Nuclear Power Systems-Water Reactor (Stevenson, WA: TMS), pp. 143-155, 2003.
[4] Y.S. Lim, D.J. Kim, S.W. Kim and H.P. Kim, Crack growth and cracking behavior of Alloy 600/182 and Alloy 690/152 welds in simulated PWR primary water, Nucl. Eng. Tech. Vol. 51, pp. 228-237, 2019.
[5] Y.S. Lim, D.J. Kim, S.W. Kim, S.S. Hwang and H.P. Kim, Characterization of internal and intergranular oxidation in Alloy 690 exposed to simulated PWR primary water and its implications with regard to stress corrosion cracking, Mater. Charact. Vol. 157, 109922, 2019.
[6] W. Kuang, M. Song and G.S. Was, Insights into the stress corrosion cracking of solution annealed alloy 690 in simulated pressurized water reactor primary water under dynamic straining, Acta Mater. Vol. 151, pp. 321-333, 2018.
[7] T. Moss, W. Kuang and G.S. Was, Stress corrosion crack initiation in Alloy 690 in high temperature water, Curr. Opin. Solid State Mater. Sci. Vol. 22, pp. 16-25, 2018.